Q. J. R. Meteorol. Soc. (1992), **118**, pp. 365–394 551.513.1:551.513.5

Upper tropospheric equatorial waves in ECMWF analyses

By WILLIAM J. RANDEL

National Center for Atmospheric Research, Boulder, CO* 80307

(Received 21 March 1991; revised 9 October 1991)

SUMMARY

Tropical wind fields from the European Centre for Medium-range Weather Forecasts operational analyses are analysed to search for equatorially trapped waves in the upper troposphere. Data are studied for 1980–87. Zonal wind spectra show a predominance of power at low zonal wave numbers and low frequencies; these data do not show distinct spectral peaks corresponding to eastward-propagating Kelvin waves or westward-propagating equatorially-trapped Rossby waves. The zonal wind spectra do show episodic evidence for westward-propagating 5-day zonal wave-1 features with maxima over the equator; these are likely related to Rossby normal-mode oscillations previously reported.

Meridional wind spectra show a predominance of westward-propagating power in the 6- to 10-day-period range, primarily concentrated in zonal waves 4–7. Enhanced meridional wind activity at the equator occurs episodically in time, with events persisting for one to several months duration. Wave packets are longitudinally localized, with preferred occurrence over the eastern Pacific Ocean. Most cases show evidence of meridional wind maxima in the tropics, suggesting a degree of equatorial trapping. The horizontal structure of these oscillations is that of mixed Rossby–gravity waves, although they are not necessarily centred directly over the equator. These waves have largest amplitudes in the upper troposphere, showing weak coherence with the surface; they appear to be fundamentally distinct from fast 4- to 5-day Rossby–gravity waves observed in the western Pacific.

A detailed study of a group of intense Rossby–gravity waves observed over the eastern Pacific during August–September 1985 is presented; the reality of these features is confirmed in direct rawinsonde observations. Correlations are found between bursts of equatorial wave activity and enhanced meridional momentum fluxes from the subtropics, suggesting extratropical forcing as at least one mechanism for their generation. The waves are also strongly coupled to the upper tropospheric zonal wind field, which likely accounts for their longitudinal and temporal confinement.

1. INTRODUCTION

This paper presents an observational study of travelling waves in the near-equatorial upper tropospheric wind field, as revealed in operational analyses produced by the European Centre for Medium-range Weather Forecasts (ECMWF) over the years 1980–87. The initial motivation for this work was to obtain wave spectra from 'observations' to make comparisons with upper tropospheric waves found in the National Center for Atmospheric Research (NCAR) Community Climate Model (CCM). Boville and Randel (1992) have used several high vertical resolution CCM simulations to study the behaviour of equatorially-trapped waves and their effects on the zonal mean flow as they propagate vertically into the stratosphere; of some concern to that study was the realism of the spectrum of wave forcing in the model upper troposphere. In an attempt to answer that, wind fields from eight years of ECMWF data have been analysed, and results are presented here on equatorial wave variability found in those data.

A review of the literature on travelling waves in the upper troposphere yields wave parameters (such as wave amplitude, period and zonal wavelength) that are derived from a limited time sample of tropical Pacific rawinsonde observations (Yanai and Maruyama 1966; Yanai and Murakami 1970; Nitta 1970; Wallace 1971; Maruyama 1979) or from short time samples of tropical analyses (Zangvill and Yanai (1980) use June–August 1967 data; Yanai and Lu (1983) use June–August 1967 and 1972 data). The wave parameters quoted in those studies are often used for benchmark values to test the generation mechanism of the waves (e.g. Itoh and Ghil 1988), or for input into mechanistic models of the stratospheric quasi-biennial oscillation (QBO) (Holton and Lindzen 1972;

* The National Center for Atmospheric Research is sponsored by the National Science Foundation.

Dunkerton 1985). Space–time spectral analyses of the ECMWF data show somewhat different results, although in restrospect it is not difficult to see why: waves in the western Pacific are not representative of all longitudes, and there is considerable seasonal and interannual variability in wave behaviour. The results presented here are based on a long sampling record of global analyses, and hence provide spectra that are more representative of true space–time variability.

The purpose of this work is to make a systematic study of observed tropical wave variability in the upper troposphere, using the long data base provided by the ECMWF analyses. We follow a methodology of using space–time spectral analyses to isolate spectral peaks associated with travelling waves in the data. Wave structures are then examined for time periods when such spectral peaks are strongest. A case study is presented for a particularly strong Rossby–gravity wave event observed in these data, with focus on understanding the wave generation mechanisms. Similar wave structures are found in simulations using the NCAR Community Climate Model (CCM1), and brief comparisons with the ECMWF data are shown.

The ECMWF global analyses used here result from a four-dimensional assimilation of available data using first-guess fields generated by the ECMWF forecast model. These assimilated fields are then 'initialized' to emphasize the slow, meteorologically significant components and damp the (spurious) fast gravity waves (which have periods less than 1 day). Assimilation of wind fields in the tropics is a particularly difficult task because of: (1) the lack of a dense network of direct wind observations, (2) delicate mass–wind balances in the tropics that make the use of geopotential or temperature data problematic, and (3) the importance of diabatic processes which are difficult to include properly in the forecast model and initialization scheme. As a result, the quality of tropical wind fields obtained in this manner is of some concern. For example, Trenberth and Olson (1988) find significant differences in the tropics between analyses produced by the ECMWF and those produced by the National Meteorological Center (NMC), although many of the same observations are included in both schemes, and the analysis techniques are fundamentally similar. Another potential problem is that any equatorial wave modes uncovered in analysis of these data might be purely an artifact of the forecast model used to assimilate the observations. Cats and Wergen (1982) showed that substantial aliasing of equatorial wave modes can occur in (an early version of) the ECMWF operational scheme, and suggest that spectra be interpreted with caution. We have therefore made extensive comparisons between the ECMWF fields and equatorial rawinsonde observations (RAOBs). These RAOB comparisons demonstrate that the travelling waves identified here are true atmospheric oscillations, not a result of the assimilation scheme.

In section 2 we discuss the ECMWF data and our analysis techniques. In section 3 we present space–time spectra that reveal the seasonal and interannual variability of travelling waves in the tropical wind fields. The zonal wind spectra exhibit a majority of power in the lowest resolved frequencies, and there is a lack of notable spectral peaks. These data do not show evidence in the zonal winds of eastward-propagating Kelvin waves or westward-propagating equatorial Rossby waves in the 10- to 20-day time scale identified in Yanai and Lu (1983); we do note the episodic occurrence of a westward-propagating 5-day zonal wave-1 feature that has characteristics consistent with a global normal-mode Rossby wave.

The upper tropospheric meridional wind spectra show maxima for westward-propagating zonal waves 4–7 with 6- to 10-day periods. Such spectral peaks occur episodically in time, with a duration of one to several months. The events are also longitudinally localized; there is a preference for westward-propagating waves to occur over the eastern Pacific Ocean during August–September. The structure of the winds for individual cases

is examined. Most cases show low-latitude maximum in meridional winds which suggests a degree of equatorial trapping. For some other events the meridional winds maximize away from the tropics, suggesting that they are extensions of travelling waves in mid latitudes. The horizontal structure of the equatorially trapped waves is that of mixed Rossby–gravity modes, although the patterns are not always situated symmetrically with respect to the equator (possibly due to the effects of background winds).

The 6- to 10-day-period Rossby–gravity waves discussed here exhibit maximum amplitudes in the upper troposphere, and weak coherence with the near-surface layers of the atmosphere (an exception to this statement may be found over South America, as discussed in section 4(c)). As a consequence, they likely do not organize low-level moisture convergence, and hence are probably not strongly coupled to convective activity. Also, the preferred location of these waves over the eastern Pacific Ocean is a region of general subsidence, where convective activity is small. This aspect of these waves appears to be fundamentally distinct from fast 4- to 5-day Rossby–gravity waves observed in the western Pacific (Liebman and Hendon 1990), and 'easterly waves' observed in the eastern Atlantic (Burpee 1972) and eastern Pacific near 10°N (Tai and Ogura 1987). These latter disturbances are most coherent in the lower troposphere, and strongly coupled to convection.

Section 4 focusses on the structure of an exceptionally large group of Rossby–gravity waves observed during August–September 1985. Comparisons with RAOB data confirm that these waves are not an artifact of the assimilation model. We find a correlation of individual wave events with bursts of extratropical momentum flux from the southern hemisphere (SH), suggesting that one excitation mechanism for these waves is from lateral forcing (*in situ* dynamical growth at the expense of the background shear flow and convective coupling over South America may also be important). The equatorial waves are also strongly coupled to the background zonal winds, which likely accounts for their longitudinal and temporal confinement.

Section 5 discusses the behaviour of similar westward-propagating waves in the upper troposphere in the NCAR CCM1. The model waves show characteristics similar to those observed in the atmosphere, notably asymmetry with respect to the equator, longitudinal and temporal confinement, and coupling with the tropical zonal wind field. Results are discussed in section 6, including the implications of these data for forcing of the QBO.

2. Data and analyses

The wind data analysed here are initialized daily operational products from the ECMWF covering the eight years 1980-87. Data are available on seven standard pressure levels (1000, 850, 700, 500, 300, 200 and 100 mb), with the original archive consisting of 2.5×2.5 degree latitude–longitude grids. These grids have been converted to 7.5 by (approximately) 4.5 degree longitude–latitude grids, consistent with rhomboidal spectral truncation at wave number 15 (R15), and archived at the NCAR. Zonal Fourier coefficients based on these data form the basis of the analyses here.

It is known that there are systematic biases in the ECMWF forecast model in the tropics (Heckley 1985), and Trenberth and Olson (1988) document substantial differences between ECMWF and NMC operational tropical data. In light of these known uncertainties, it is reasonable to question the reality of transient waves in these data. Liebman and Hendon (1990) have documented 4- to 5-day Rossby–gravity waves in the tropical lower troposphere in the ECMWF data, validating the analyses with coherent oscillations observed in independent outgoing longwave radiation (o.l.r.) measurements. Here we

have made comparisons with direct RAOB wind measurements, and the observed good correlations prompt confidence in the upper tropospheric analyses. The quality of these data in the tropical lower and upper troposphere is likely due to the availability of satellite cloud-drift winds and frequent aircraft reports, respectively.

Space–time spectral analyses are performed based on the standard technique of Hayashi (1982). Direct Fourier transform in time is used to estimate the spectral coefficients, which are smoothed using a 0.065–0.245–0.380–0.245–0.065 convolution in frequency (these coefficients were calculated using a Gaussian-shaped spectral window; the frequency bandwidth is shown in Fig. 1). Sixty-day time series are used for the spectral analyses. The time means of each series are removed before analysis, and due to frequency smoothing the lowest resolved period shown is 30 days. Variability below this limit is not considered here. Horizontal grids of eastward- or westward-propagating wave components were reconstructed from the space–time coefficients using the formulae presented in Appendix B of Ziemke and Stanford (1990).

Power spectra ($P(\omega)$) are presented here using linear frequency (ω) as the dependent variable (although the corresponding wave periods are labelled on the plots). Zangvill (1977) has discussed alternative representations, suggesting that the power spectrum be multiplied by frequency ($\omega \cdot P(\omega)$) and then plotted versus the logarithm of frequency ($\ln \omega$); this convention has been used by Zangvill and Yanai (1980), Yanai and Lu (1983) and Magaña and Yanai (1991). Two problems with that approach are: (1) a varying spectral bandwidth in the diagrams, and (more importantly) (2) a representation of the spectra which suggests that the largest power is not at the lowest frequencies (especially for eyes trained by examining linear frequency spectra). Because most time series of atmospheric variables have 'red' power spectra (most power at small ω), diagrams of $\omega \cdot P(\omega)$ will always show a localized spectral maximum, although the time series may have no preferred periodicities. The spectral features analysed here are usually not absolute spectral maxima (the spectra show an overall red character), but rather relative maxima. The statistical significance of these peaks has not been assessed (by comparison with a red background spectrum, for instance), but rather the focus is on the waves' spatial and temporal characteristics.

3. Spectral analyses of ECMWF tropical wind data

Figure 1 shows wave-number frequency diagrams of eight-year-ensemble spectral power density for the zonal and meridional wind components at 200 mb over the equator. Calculations are made for data over January–February and August–September. The zonal wind spectra show maximum power in the lowest zonal wave numbers ($\approx$1–2) and lowest frequencies, and there is an absence of any notable spectral peaks. There is slightly more power in low-frequency eastward-moving waves: the overall signature is consistent with quasi-stationary or slowly eastward-moving variance. Similar zonal wind spectra are found at other levels throughout the troposphere (not shown here). The 200 mb meridional wind spectra in Fig. 1 show a predominance of power for westward-moving zonal waves $\approx$4–7 (zonal wavelengths 6–10 000 km) in the period range 6–10 days (maxima near 7–8 days). The data in Fig. 1 are eight-year averages—individual months data may or may not exhibit distinct peaks, as shown below.

Unlike the zonal wind spectra, the meridional wind power changes character between the upper and lower troposphere. Figure 2 shows August–September meridional wind spectra at 500 and 850 mb, demonstrating a shift toward higher-frequency waves in the lower troposphere (periods centred near 5 days). The character of these fast 4- to 5-day

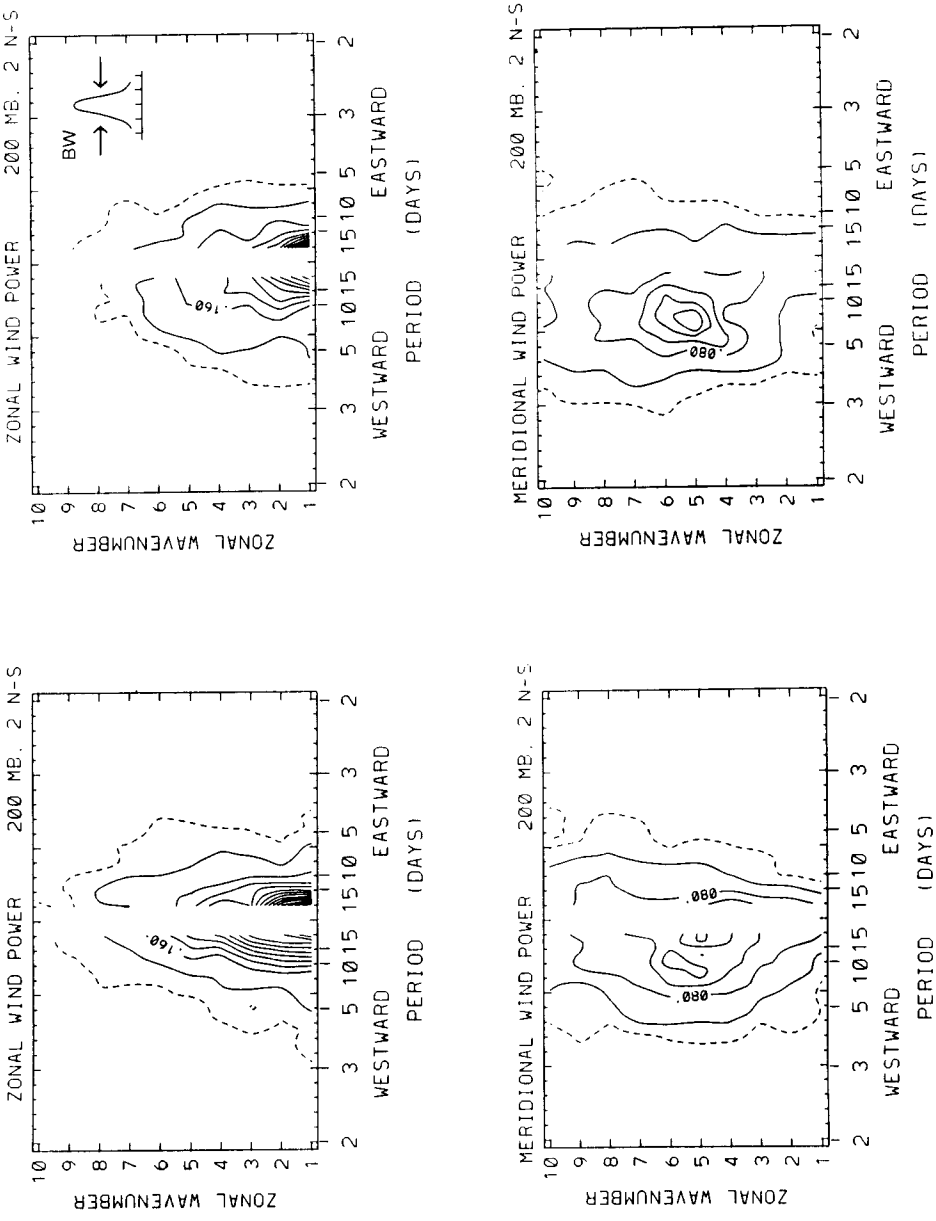

Figure 1. Ensemble 8-year average (1980–87) zonal wave number–frequency spectra of zonal (top) and meridional (bottom) winds over the equator at 200 mb. Left panel shows data over January–February, and right panel August–September. Spectral-density contours are 0.08 (top) and 0.04 (bottom) $m^2 s^{-2} \times \Delta\omega^{-1}$, and the dashed lines are one-half the lowest contour level. The spectral bandwidth (BW) is indicated in the upper-right panel.

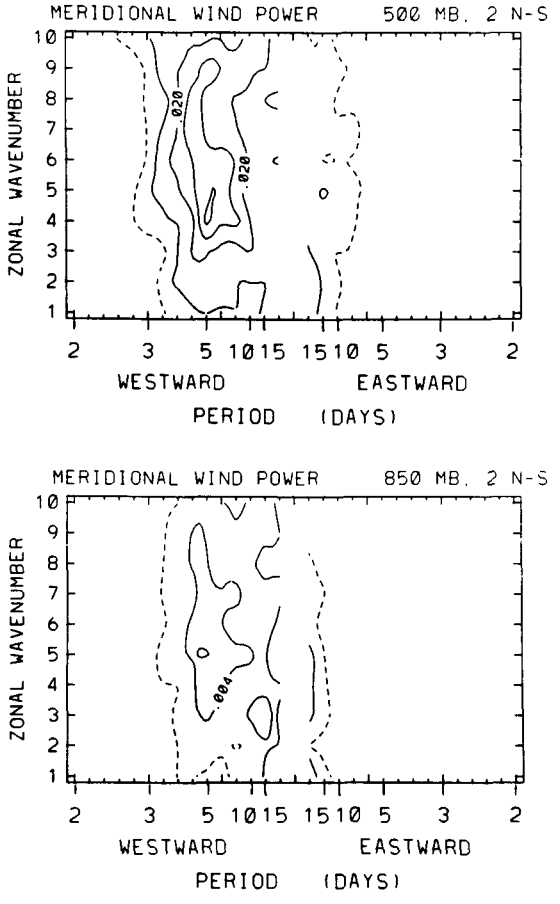

Figure 2. Wave number–frequency spectra of meridional winds over the equator during August–September 1980–87 at 500 mb (top) and 850 mb (bottom). Contour intervals are 0.01 and 0.004 $m^2 s^{-2} \times \Delta\omega^{-1}$, respectively.

waves in the ECMWF data have recently been analysed by Liebman and Hendon (1990); they show these spectral signatures to result from mixed Rossby–gravity modes which are most coherent in the lower troposphere, with largest amplitudes over the tropical western Pacific Ocean. These fast waves contribute a relatively small fraction of the meridional wind variance in the upper troposphere (cf. Fig. 1), and we focus our study on the latter region.

Although the ensemble zonal wind spectra show no distinct peaks, data for individual months were searched for the planetary wave modes identified in Zangvill and Yanai (1980) and Yanai and Lu (1983), namely 10- to 20-day eastward-propagating Kelvin waves and westward-moving equatorially-trapped Rossby modes. Figure 3 shows spectra for individual months over 1984–85 of the zonal wave-1 component of zonal wind at 200 mb over the equator. These spectra were calculated from overlapping 60-day time series centred on each month. The majority of variance in Fig. 3 is found in the lowest frequencies, skewed towards eastward propagation. There is little evidence in Fig. 3 of distinct maxima for 10- to 20-day-period eastward or westward modes (Kelvin or equatorially-trapped Rossby waves, respectively) that were identified in the study of Yanai and Lu (1983). It is possible that such modes may be present in these data, but are smeared into lower frequencies by non-stationary behaviour. There is evidence in

Fig. 3 of small-amplitude westward-propagating waves with a period near 5 days, which reoccur episodically (April–June 1984, January–April 1985). The 200 mb meridional structure of the wave-1 zonal wind spectra is shown in Fig. 4(a), calculated from data over May–June 1984. There is a maximum centred over the equator near westward period 5 days with amplitude confined within approximately 10°N–S. Similar patterns are found throughout the troposphere (Fig. 4(b)): this 5-day wave exhibits significant amplitude and statistical coherency all the way to the surface. The spectral power for

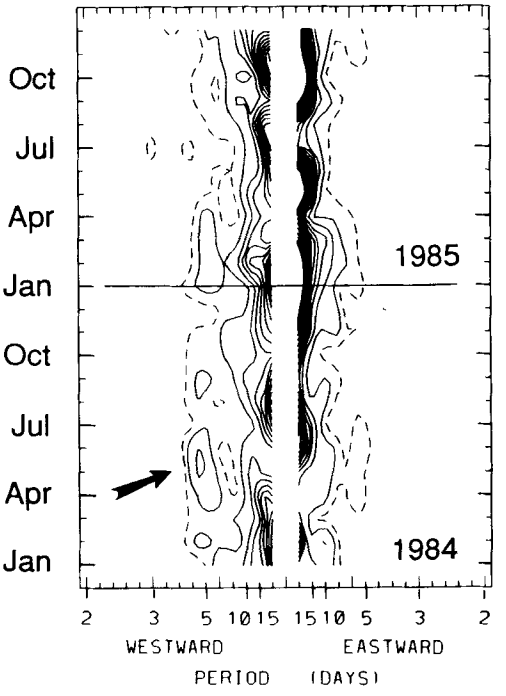

Figure 3. Power spectra for zonal wave-number-1 zonal wind fluctuations over the equator at 200 mb for data over 1984–85. Spectra are calculated from overlapping 60-day time series centred on each month. Contour interval is $0.10\,m^2s^{-2} \times \Delta\omega^{-1}$. Arrow in 1984 denotes the time period analysed in Fig. 4.

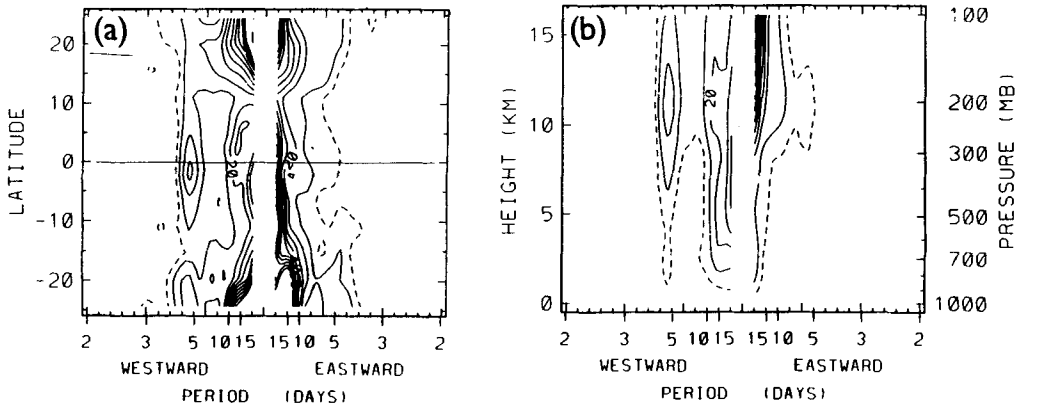

Figure 4. (a) Latitude–frequency power spectra at 200 mb of zonal wave-number-1 zonal wind oscillations calculated from data over May–June 1984. Contour interval (solid lines) is $0.10\,m^2s^{-2} \times \Delta\omega^{-1}$. (b) Height–frequency section at the equator for the same data.

this mode corresponds to an amplitude near 1 m s^{-1} at 200 mb and 0.5 m s^{-1} at the surface. The 5-day zonal winds are in phase both horizontally and vertically. Spectral peaks for a westward-moving 5-day wave 1 were observed also in Yanai and Lu (1983), who identify it with free global normal-mode Rossby waves (which theoretically should possess small horizontal and vertical phase variations near the equator). Tsay (1974) observed a similar feature in an early version of the NCAR CCM.

Although the zonal winds for such a mode have a maximum near the equator, geopotential-height anomalies should maximize in mid latitudes (there should also be perturbation zonal winds in high latitudes). Zonal wave-1 geopotential data indeed exhibit a spectral peak for this 5-day feature. The global structure of this mode over 1000–1 mb is displayed in Fig. 5(a), based on data obtained from the NMC. These data are used to extend the analyses above 100 mb; the NMC and ECMWF data yield virtually identical results over 1000–100 mb. For reference, the zonal winds for this time period

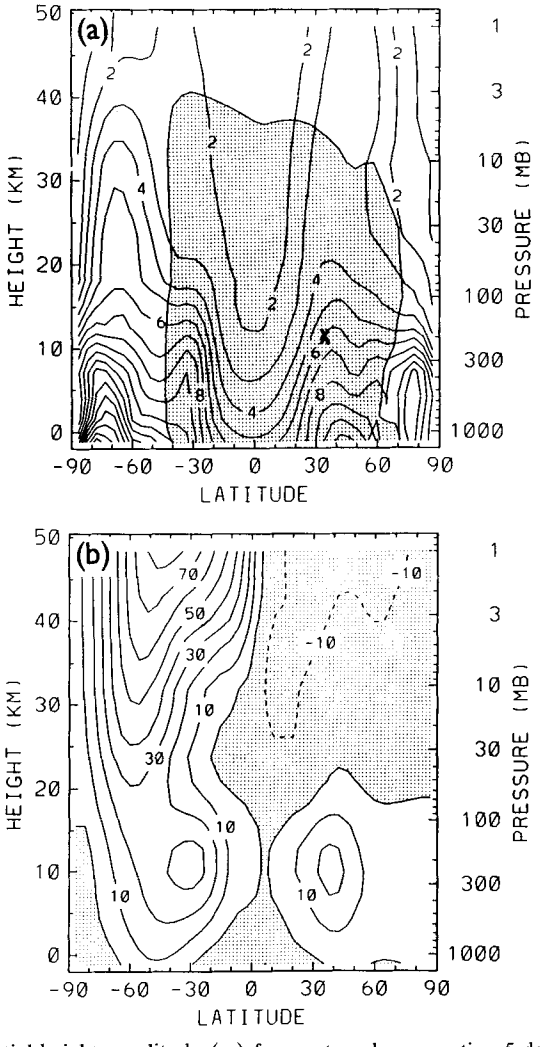

Figure 5. (a) Geopotential-height amplitude (m) for westward-propagating 5-day wave during May–June 1984. Amplitudes have been multiplied by $(P/1000\,\text{mb})^{1/2}$ to remove the effect of density stratification. The shaded region denotes statistical coherence above the 5% significance level with respect to a reference position at 200 mb, 33°N. (b) Zonal mean winds (m s^{-1}) for May–June 1984.

are shown in Fig. 5(b). Figure 5(a) shows the geopotential-height amplitude, calculated as the square root of twice the spectral power summed over a frequency band centred on 5-days (westward). The amplitudes are further multiplied by $(P/1000\,\mathrm{mb})^{1/2}$, to remove the effect of density stratification. The stippled region denotes where the mode is statistically coherent (above the 5% significance level) with a reference position at 33°N, 200 mb. This cross-section shows height maxima in the troposphere and stratosphere near 30–40° in each hemisphere, a minimum at the equator, and strong coherence from the surface to above 10 mb. The geopotential wave (not shown) is approximately in phase both horizontally and vertically over the entire coherent region in Fig. 5(a). Venne (1989, his Fig. 2) has isolated a similar structure from a long time series of NMC data. This overall structure agrees well with the idealized normal-mode calculations for the 5-day wave shown by Salby (1981, his Fig. 6). These clear structural signatures, along with the similar wave period for each of the 'events' seen in Fig. 3, makes rather certain identification of this feature as a normal-mode oscillation.

Figure 6 shows power spectra for zonal wave 5–6 meridional wind fluctuations over the entire record 1980–87, again calculated from overlapping 60-day time series centred on each month. Strong episodes of westward-propagating wave activity are evident with periods of 6–10 days; the exact central frequencies and bandwidths of individual maxima are variable. These bursts of activity typically persist for several months at a time (e.g. February–May and October–December 1984). Although the episodes are not regularly occurring, several strong events are observed during the northern hemisphere (NH) summer months July–October (e.g. 1981, 1982, 1985, 1986, 1987). There are also several long-lasting episodes of enhanced low-frequency variance (September 1981–March 1982; September 1986–March 1987). There is little evidence in Fig. 6 of systematic changes in wave spectra during the El Niño warm episodes of 1982–83 and 1987.

The meridional structure of the wave 5–6 meridional wind variance at 200 mb is shown in Fig. 7 for six cases identified from the spectra in Fig. 6. Each diagram shows a spectral maximum over the equator for westward-propagating waves with periods in the range 5–15 days; the detailed meridional structures are quite different for each case, however. Most cases show a latitudinal maximum in meridional wind variance near the equator, suggesting a degree of meridional trapping. Some maxima are centred directly over the equator (cases 1 and 2), while others show maximum variance somewhat south of the equator (cases 3, 4 and 6); this latter behaviour is also seen for the August–September 1985 case discussed below. Case 5 shows no variance maximum near the equator. Rather, the patterns suggest that the equatorial variance is an extension of that in the NH subtropics. Such patterns are consistent with the meridional propagation of mid-latitude waves towards the equator; theory suggests deeper penetration (and perhaps cross-equatorial propagation) for westward-propagating waves (e.g. Karoly 1983).

The horizontal structure of the equatorially-trapped waves is illustrated in Fig. 8 for case 1 (November–December 1983). The westward-propagating wave variance maximizes over the central eastern Pacific Ocean during this time, and Fig. 8 focusses on that region. The vectors in Fig. 8 were constructed by regressing the zonal and meridional wind components at each latitude/longitude upon a reference time series of the meridional wind at 240°E, 2°S. The fields were first filtered to retain only westward-propagating waves of periods 5–15 days. The horizontal patterns in Fig. 8 are signatures of a mixed Rossby–gravity wave situated symmetrically over the equator (cf. Matsuno 1966). The other equatorially-trapped structures in Fig. 7 have similar Rossby–gravity wave signatures; for cases 3, 4 and 6 the entire patterns are shifted south of the equator (as shown for August–September 1985 below). Root-mean-square (r.m.s.) values of the meridional winds at 200 mb for these modes are of the order 1–4 $\mathrm{m\,s^{-1}}$.

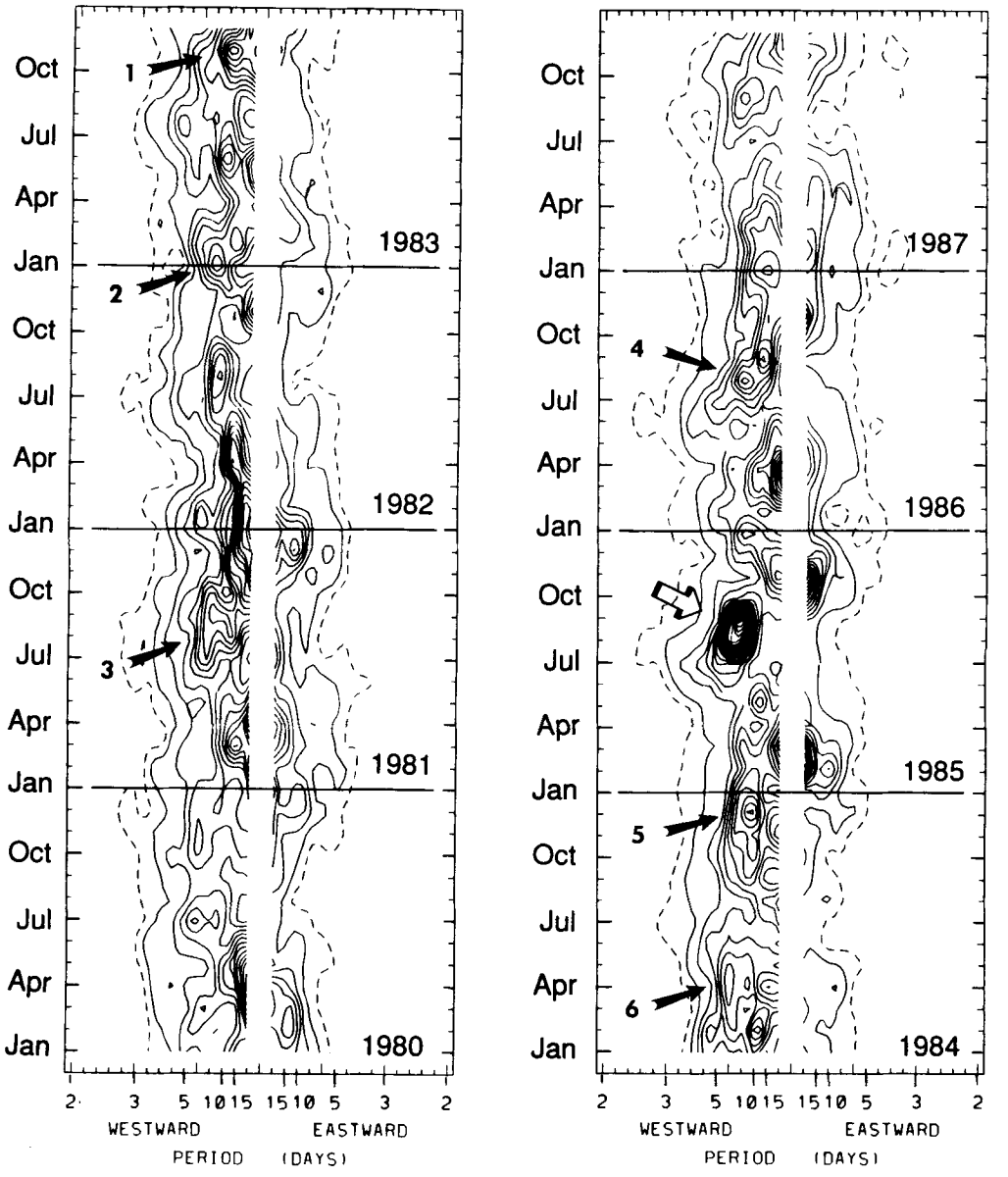

Figure 6. Power spectra for zonal wave-number 5–6 meridional wind fluctuations over the equator at 200 mb, for the entire data record 1980–87. Spectra are calculated from overlapping 60-day time series centred on each month. Contour interval is $0.06\,m^2s^{-2} \times \Delta\omega^{-1}$. Numbered arrows refer to the cases analysed in Fig. 7. Highlighted arrow in 1985 shows the case study analysed in section 4.

Figure 9 shows height–frequency sections at the equator of wave 5–6 power for cases 1 and 3 (other cases are similar). The 5- to 15-day variance is a maximum near 200 mb, with weak values below 700 mb. The meridional wind in the 5- to 15-day frequency band exhibits statistical coherence over 700–100 mb (not shown here), notably *not* all the way to the surface. Both sections in Fig. 9 show weak secondary maxima for westward-propagating 4- to 5-day-period waves. In the lower troposphere the 4- to 5-day variance is nearly as large as that for the lower-frequency waves. In the upper troposphere, however, the amount of variance for the faster waves is insignificant.

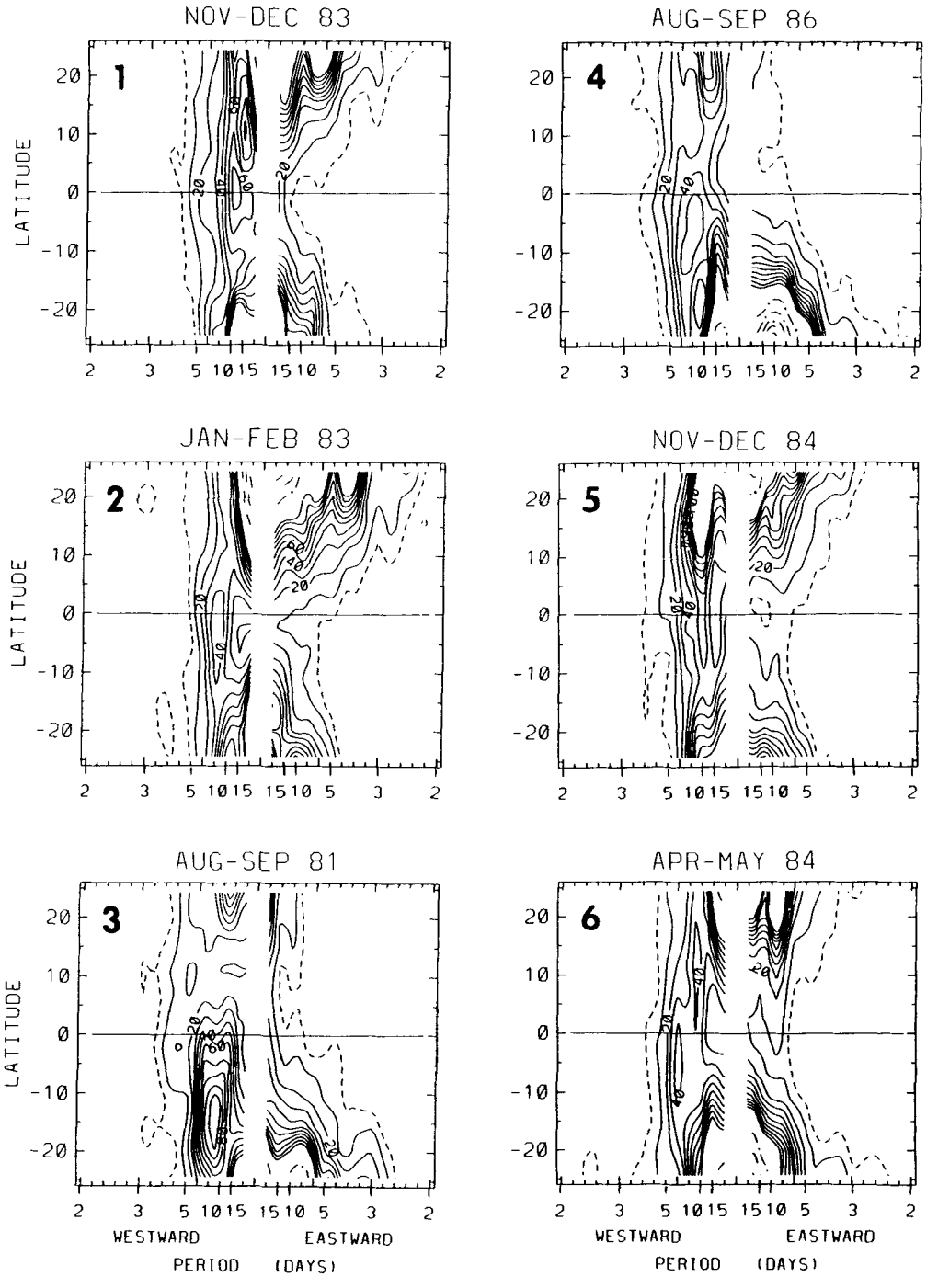

Figure 7. (a) Latitude–frequency power spectra at 200 mb for zonal wave-number 5–6 meridional wind fluctuations for six cases chosen from the spectra in Fig. 6. Time periods are labelled and correspond to the numbered arrows in Fig. 6. Contour interval (solid lines) is $0.10\,m^2 s^{-2} \times \Delta\omega^{-1}$. Dashed lines are one half the lowest contour interval, and dot-dashed contours are multiplied by ten.

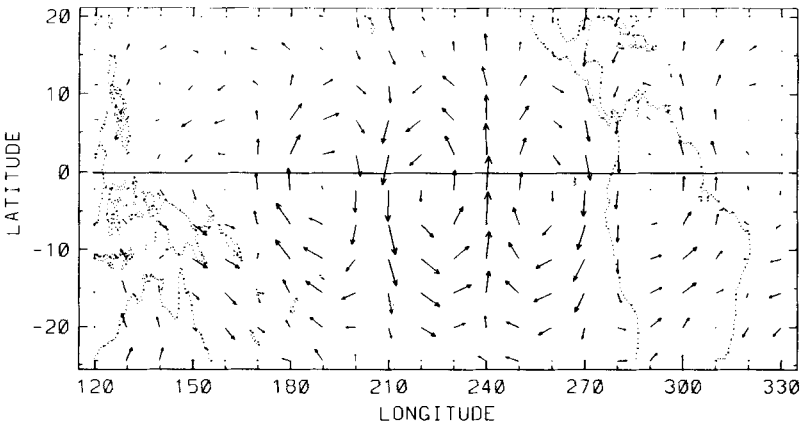

Figure 8. Latitude–longitude diagram of the horizontal structure of westward-propagating fluctuations with periods 5–15 days for data over November–December 1983 (case 1). Components of each vector are calculated as regressions upon a reference time series of meridional wind at 240°E, 2°S. The longest vector is 1.9 $m s^{-1}$.

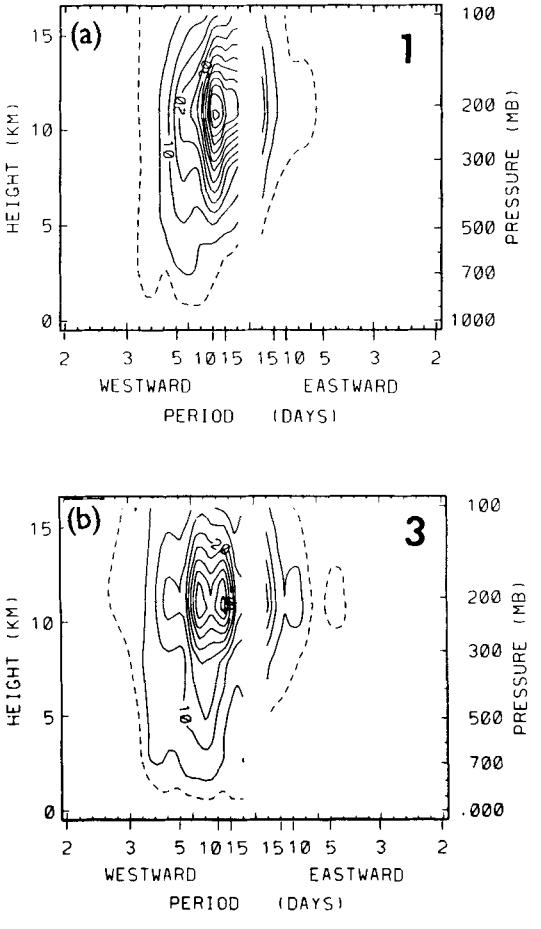

Figure 9. Height–frequency spectra at the equator of wave 5–6 meridional winds for (a) case 1 and (b) case 3 (see Figs. 6–7). Contour interval is 0.05 $m^2 s^{-2} \times \Delta\omega^{-1}$.

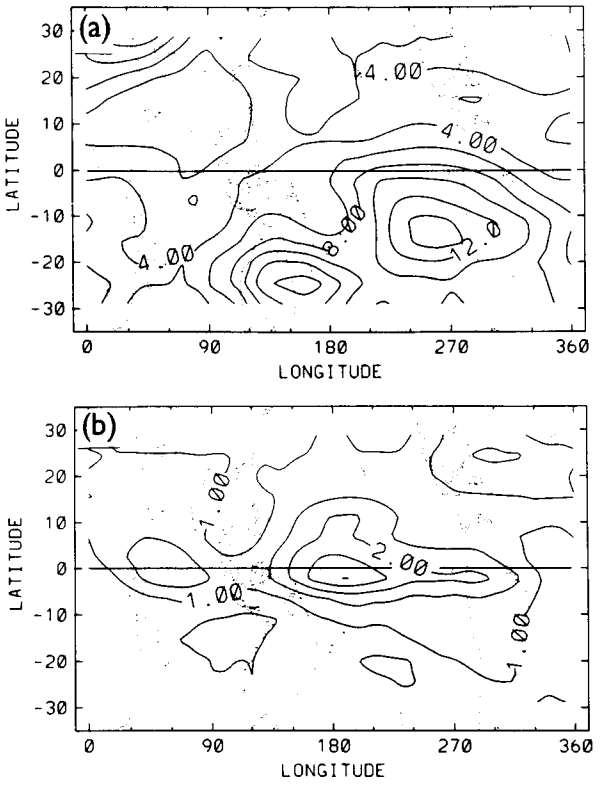

Figure 10. Latitude–longitude sections at 200 mb of the meridional wind variance for westward-propagating fluctuations in the period range (a) 6–15 days and (b) 3–5 days for data over August–September 1981 (case 3). Contour intervals are (a) $2\,m^2\,s^{-2}$ and (b) $0.5\,m^2\,s^{-2}$.

Figure 10 shows horizontal maps of the 200 mb meridional wind variance for August–September 1981 (case 3), synthesized for two nonoverlapping frequency bands: 6–15 days westward and 3–5 days westward (these include full zonal resolution and thus can indicate longitudinally-localized variability). The 6- to 15-day variance (Fig. 10(a)) is a maximum in the western hemisphere, with peak values over 10–20°S. The 3- to 5-day variance (Fig. 10(b)) is situated symmetrically over the equator, with maximum values near the dateline. This latter pattern is consistent with the 4- to 5-day Rossby–gravity modes discussed in Liebman and Hendon (1990) and Hendon and Liebman (1991), which they show to maximize near the dateline, and also with the pioneering studies of Yanai and Maruyama (1966), Yanai and Murakami (1970) and Nitta (1970), who base their analyses on central Pacific rawinsonde observations. Inspection of the spectra in Fig. 9, and the variance maps in Fig. 10, shows that the 4- to 5-day waves contain a relatively minor component of the upper tropospheric variance when viewed in a zonally-averaged sense, although they may be important locally.

4. Wave event of August–September 1985

(*a*) *Wave structure*

By far the most intense maximum observed in the meridional wind spectra in Fig. 6 occurred during August–September 1985. Figure 11(a) shows a Hofmöller diagram

of the 200 mb meridional wind at 2°S during that time period. Westward-propagating waves with local maxima in excess of $10\,m\,s^{-1}$ are observed, mainly in the longitude band 150°–300° (in the eastern Pacific Ocean). The predominant zonal wavelength is near 7–8000 km, and local wave periods are near 6–8 days. The zonal phase velocity determined from Fig. 11(a) is near $10–15\,m\,s^{-1}$ westward, and there is evidence of eastward group velocity of order $15\,m\,s^{-1}$ (as indicated for the latter half of September in Fig. 11(a)).

Figure 11(b) shows a space–time spectrum of the data in Fig. 11(a). Also indicated is a dispersion curve fit to the relation

$$\frac{N}{\omega^2}(\beta + \omega k) = m \tag{1}$$

corresponding to a Rossby–gravity wave packet with specified vertical structure (e.g.

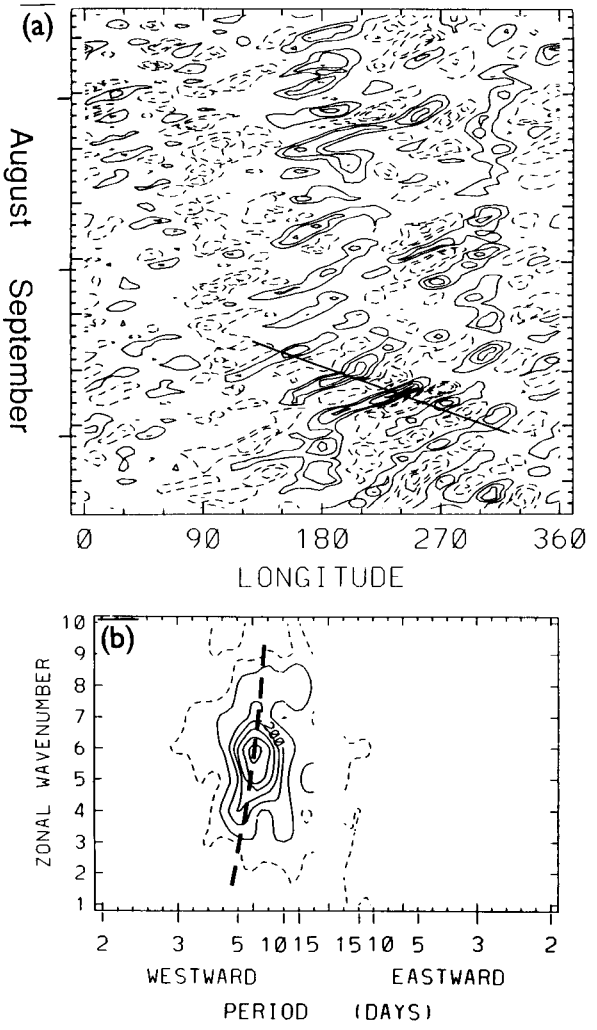

Figure 11. (a) Hofmöller diagram of the meridional wind at 200 mb, 2°S over 90 days centred on August–September 1985; no space or time filtering has been applied. Contour interval is $4\,m\,s^{-1}$, with zero contours omitted. The straight line in the latter half of September denotes a wave packet with eastward group velocity near $15\,m\,s^{-1}$. (b) Space–time spectral signature of the data in (a). Contour interval is $0.10\,m^2\,s^{-2} \times \Delta\omega^{-1}$. Heavy dashed line corresponds to a Rossby–gravity wave dispersion curve using an equivalent depth of 16 m, as discussed in text.

Pedlosky 1979, section 8.5). Here $N = 1.0 \times 10^{-2}\,s^{-1}$ is the upper tropospheric static-stability parameter, $\beta = 2.3 \times 10^{-11}\,m^{-1}s^{-1}$, ω is the angular frequency, k the dimensional zonal wave number, and m is a constant related to the vertical structure. This constant m is chosen here to fit the 6.0 day wave 6 maximum in Fig. 11(b), and is equal to $7.9 \times 10^{-4}\,m^{-1}$. A shallow-water equivalent depth h may be assigned to this value of m by the relation $h = (N^2/gm^2)$, with $g = 9.8\,m\,s^{-2}$, resulting in a value of h of about 16 m. The corresponding zonal phase speed of this shallow-water mode is $c = -(gh)^{1/2}$ approximately $-12\,m\,s^{-1}$, very close to the value observed. This value of h is an order of magnitude smaller than that calculated by Yanai and Lu (1983, Table 2) for the 5-day Rossby–gravity mode. Liebman and Hendon (1990, Fig. 8) calculate estimates of h ranging over several orders of magnitude, with 5- to 10-day 'central Pacific' waves having h of order 10 m, similar to that found here.

Figure 12(a) shows a latitude–longitude cross-section of the meridional wind variance synthesized from the frequency band of westward-propagating waves with 5- to 10-day periods. There is a maximum over the eastern Pacific Ocean and South America, with the variance centre located south of the equator near 5–10°S; similar variance patterns were found during August–September 1981 (Fig. 10(a)). Patterns similar to that seen in Fig. 12(a) are found at 100 and 300 mb, but the 500 mb maximum is located much more symmetrically about the equator. Figure 12(b) shows a map of the time-averaged zonal

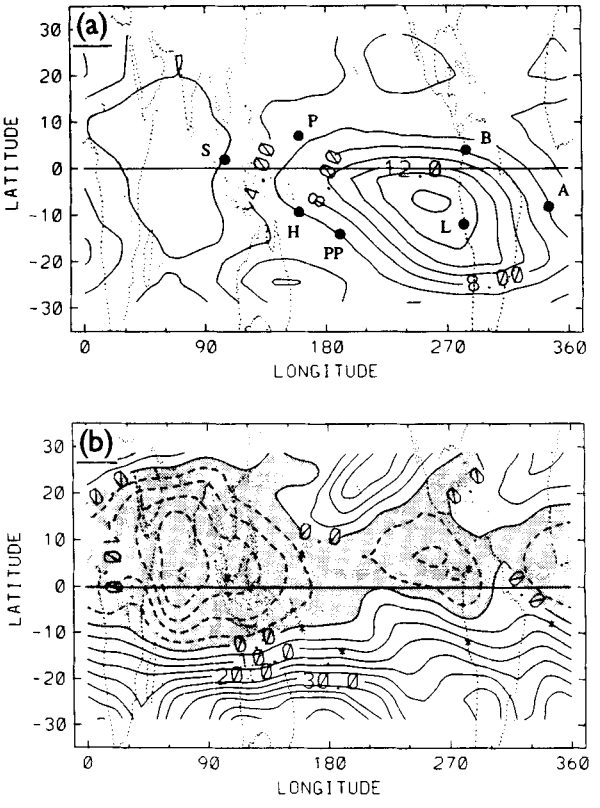

Figure 12. (a) Latitude–longitude map of the meridional wind variance for westward-propagating zonal waves 4–7 with periods 5–10 days, calculated from data over August–September 1985. Contour interval is $2\,m^2s^{-2}$. Dots denote RAOB station locations, abbreviated as: S (Singapore), P (Ponape), B (Bogota), H (Honiara), PP (Pago Pago), L (Lima), A (Ascension). (b) 200 mb zonal wind averaged over August–September 1985. Shaded winds are easterly.

wind during this period. Comparison with Fig. 12(a) shows that the waves maximize in a region of weak westerly zonal winds ($\langle u \rangle$); considering the observed zonal phase velocities (c) near -10 to $-15\,\mathrm{m\,s^{-1}}$, these waves do not have a critical line ($\langle u \rangle - c = 0$) in this region, although their intrinsic phase velocity becomes small north of the equator where $\langle u \rangle$ is between -5 to $-10\,\mathrm{m\,s^{-1}}$. The meridional e-folding distance, l, for a Rossby–gravity mode in a motionless background is given by $l = (N/\beta m)^{1/2}$, about 7° latitude for the wave parameters considered above (this is the distance over which the wave amplitude will fall to a value 1/e of its maximum). The meridional structure shown in Fig. 12(a) has a substantially broader e-folding distance (of order 30° latitude). This broader scale may be related to the background westerlies seen in Fig. 12(b); Zhang and Webster (1989) show a marked reduction in meridional trapping for such a case.

Figure 13 shows patterns of the 200 mb horizontal wind field associated with the westward-propagating waves, constructed by regressing the wind components upon a reference time series of the meridional wind at 260°E, 7°S (near the maximum in Fig. 12(a)) in an identical manner to that for Fig. 8. The horizontal patterns in Fig. 13 are signatures of a Rossby–gravity mode, with the entire patterns shifted somewhat south of the equator (the approximate axis of symmetry is indicated in Fig. 13).

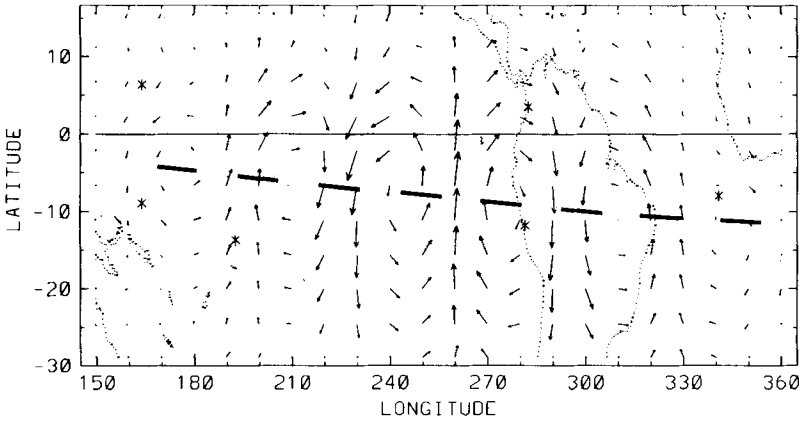

Figure 13. Latitude–longitude diagram of the horizontal structure of the westward-propagating fluctuations at 200 mb highlighted in Figs. 11–12. Components of each vector are calculated as regressions upon the reference time series of meridional wind at 260°E, 7°S. The longest vector represents $4.5\,\mathrm{m\,s^{-1}}$. The heavy dashed line indicates the approximate axis of symmetry for these waves.

Figure 14 shows a cross-section of the vertical phase structure of this mode at 7°S, calculated as correlations of the meridional wind with respect to a reference time series at 200 mb and 270°E. This shows an in-phase vertical structure, coherent only above 500 mb to the west of the wave-packet centre. The eastern portion of the wave has a deeper vertical structure, extending nearly to the surface. Note that this deeper structure occurs over and to the east of South America, possibly suggesting a coupling with convection over the continent (but not to the west). This vertical structure is discussed further below.

(*b*) *Validation in rawinsonde wind observations*

Although these modes are observed in the operational analyses, it is not clear to what degree they may be an artifact of the forecast model used to assimilate the observations. In order to determine the reality of these 6- to 8-day wind oscillations, we have made comparisons with time series of RAOB data available at NCAR. Seven

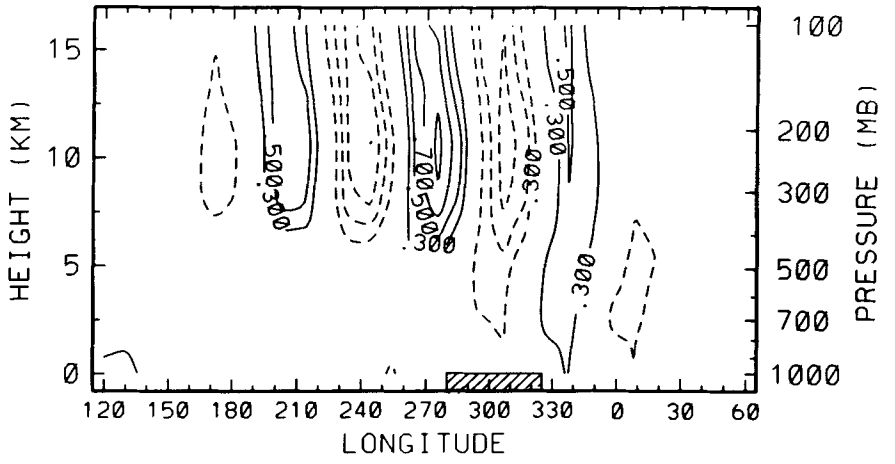

Figure 14. Vertical phase structure at 7°S of the waves shown in Fig. 13. Contours show correlations of the meridional wind with respect to a reference at 270°E, 200 mb. Contours are ±0.3, 0.5, 0.7 and 0.9. The hatched region at the bottom denotes longitudes over South America.

stations in the region of interest have been located with wind observations spanning this time period; their locations are noted in Fig. 12(a).

Figure 15 shows time series of the available RAOB meridional wind measurements at each station, along with the ECMWF wind analyses interpolated to each station location; note that there are varying amounts of missing RAOB data in these time series. Also noted in Fig. 15 are the correlation coefficients between the time series, calculated only over the days of available RAOB data. The comparisons in Fig. 15 show overall good agreement; in particular, wind oscillations of order $10\,\mathrm{m\,s^{-1}}$ are seen at each position, and the correlation coefficients are of order 0.6 or higher at each station. Note the somewhat larger-amplitude oscillations observed at station Lima in Fig. 15, in agreement with the maximum in wind variance found near there in the analyses in Fig. 12(a).

Figure 16 shows temporal power spectra for the Bogata and Lima time series shown in Fig. 15. The spectra from the ECMWF data are calculated from all 90-days' data using a lag correlation spectral-analysis technique (e.g. Chatfield (1980), chapter 7). Spectra for the RAOB data use a similar technique, but only the available data are used to calculate the lagged auto-covariance estimates. The power spectra in Fig. 16 show a distinct spectral peak near period 7 days, and there is reasonable agreement between power estimated by the analyses and that calculated from direct wind measurements. Similar agreements (not shown) are found at the other station locations.

Cross-spectral calculations were used to calculate the phase differences of the 6- to 8-day meridional wind oscillations between the separate RAOB locations. An approximate fit of these phase differences (allowing for phase shifts of 360°) is consistent with interpretation of these oscillations as westward-propagating waves with a zonal scale of approximately 60° longitude—a similar value is derived from the ECMWF analyses in Fig. 13. Overall we find good agreement between the RAOB measurements and the ECMWF analyses during this period, demonstrating that the wave structures observed in the analyses are in fact real atmospheric oscillations. Similar detailed comparisons were made for the time period April–June 1984 and good agrement is also found, leading us to believe that the spectra obtained from these analyses (e.g. section 3) are in fact representative of true large-scale variability in the upper troposphere.

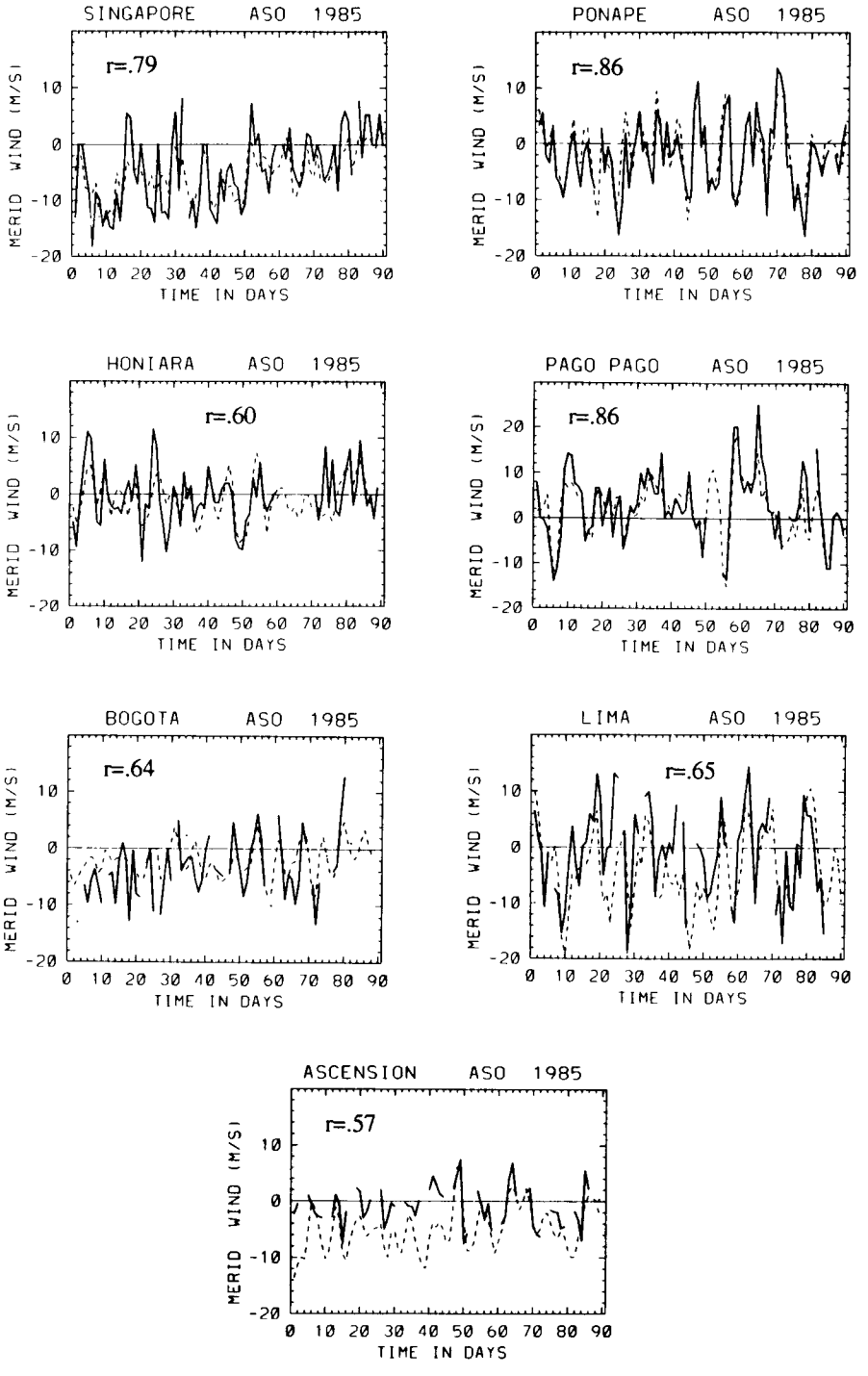

Figure 15. Time series over August–October 1985 of the 200 mb meridional wind at the RAOB stations indicated in Fig. 12(a). Solid lines are rawinsonde observations, and dashed lines are ECMWF analyses interpolated to the station locations. Missing RAOB data are not plotted. The correlation coefficient (r) between the two data is shown in each panel.

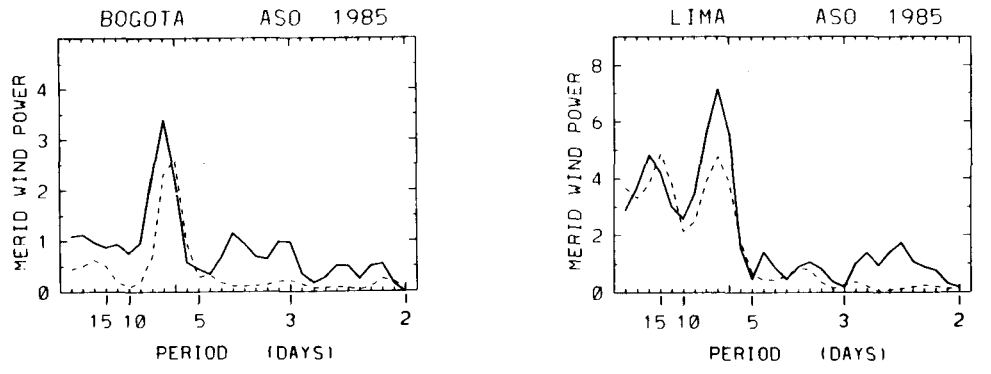

Figure 16. Temporal power spectra of the 200 mb meridional wind time series at Bogota and Lima shown in Fig. 15. Solid lines are calculated from RAOB data, dashed lines from ECMWF analyses.

(c) *Tropical wave forcing*

Possible forcing mechanisms for equatorially-trapped waves fall broadly into two categories: (1) *in situ* tropical generation, coupled to convective latent-heat release, or (2) a resonant-like response to extratropical forcings. Hendon and Liebman (1991) propose the former mechanism to be important for the fast (4–5 day) waves observed in the central Pacific, as evidenced by the waves' coupling with contemporaneous o.l.r. data (a proxy for convection). Such a mechanism is probably not the sole forcing for the upper tropospheric features detailed here, because they are not strongly coupled to the surface over much of their longitudinal domain (e.g. Fig. 14), and cannot tap the low-level moisture field (although this mechanism may be important locally over South America). We therefore look for evidence of extratropical forcing. A measure of the meridional flux of wave energy may be estimated from the meridional momentum flux uv. Partitioning the wind fields into time-mean and eddy components according to $u = \langle u \rangle + u^*$, the total momentum flux may be written as

$$uv = \langle u \rangle \langle v \rangle + \langle u \rangle v^* + u^* \langle v \rangle + u^* v^*. \tag{2}$$

The first term in Eq. (2) is constant in time. The middle two terms represent eddy fluxes of mean flow momentum, and the last term is a pure eddy-flux term. Zangvill and Yanai (1980) and Yanai and Lu (1983) analysed the zonally-averaged momentum-flux cospectra, equivalent to the last term in Eq. (2) if zonal mean fluxes are considered. Because the equatorial waves are longitudinally localized, it is most useful to analyse momentum fluxes only over the longitude region of the waves; furthermore, we find the middle two terms in Eq. (2) to be important, and include them in the momentum-flux analyses.

Figure 17 shows the time average eddy meridional momentum flux $\langle u^* v^* \rangle$ for July–September 1985. Comparison with the mean zonal winds in Fig. 12(b) shows that the extratropical SH fluxes approach closer to the equator over longitudes where the equatorial zonal winds are more westerly (in the longitude band 210–330°E). Together with the (negative) momentum flux from the SH, there is a positive maximum nearly over the equator in the region of the equatorial waves. This local maximum does not appear connected to higher-latitude maxima in the NH, and is likely due to the equatorial waves themselves (see below). Time variations of the momentum fluxes in these regions are analysed by constructing time series averaged over the shaded longitude bands indicated in Fig. 17.

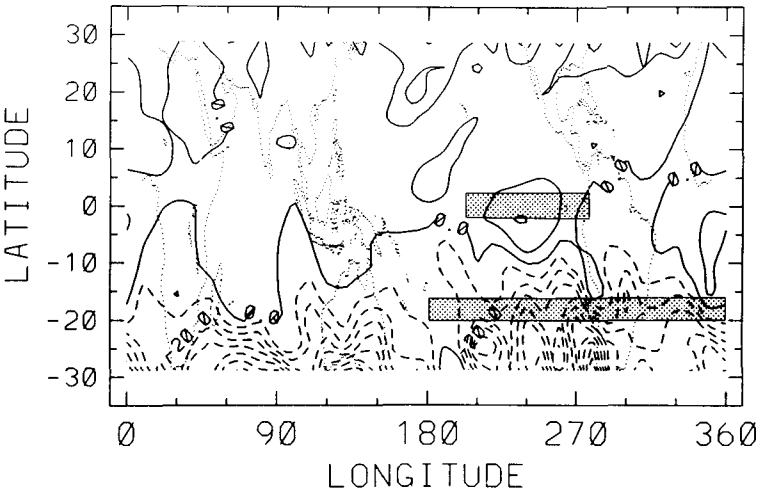

Figure 17. July–September 1985 average eddy meridional momentum flux $\langle u^* v^* \rangle$ at 200 mb. Contour interval is $10\,m^2 s^{-2}$. Shaded regions denote the averaging area for the momentum-flux time series shown in Fig. 18.

Figure 18 shows time series over June–October 1985 of the westward-propagating meridional wind variance in the eastern Pacific (area averaged over 2°N–16°S, 210–330°E; see Fig. 12(a)). This time series shows that the enhanced wave activity over July–September is actually composed of several individual wave bursts which grow and decay with a time scale of approximately 5 days; these amplitude modulations can also be seen in Fig. 11(a). Also shown in Fig. 18 are time series of the momentum fluxes across the southern boundary region indicated in Fig. 17 (dashed line), and over the equator (solid line). Features of note in Fig. 18 are: (1) enhanced momentum fluxes occur over the same general time period as enhanced equatorial wave activity (July–September)—fluxes are smaller before and after; and (2) individual peaks in equatorial wave variance are

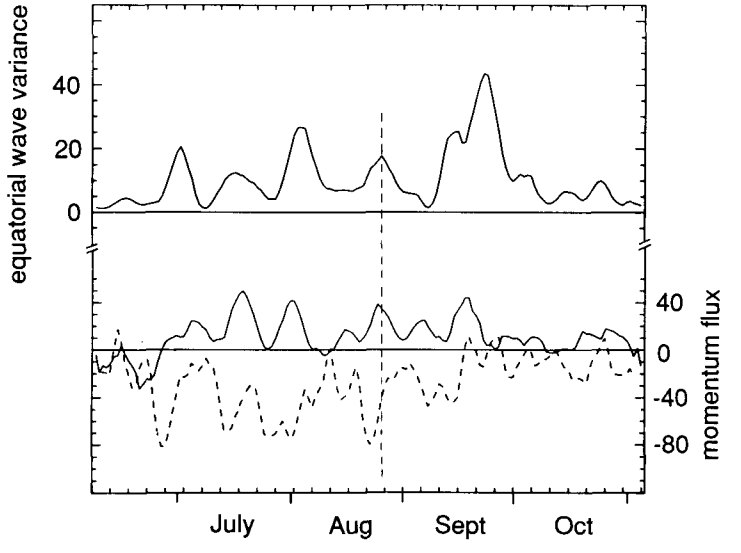

Figure 18. Top curve shows meridional wind variance for the Rossby–gravity waves isolated in Fig. 12(a), averaged over 210–330°E, 2°N–16°S. Bottom curves are time series of the meridional momentum fluxes averaged over the regions shaded in Fig. 17. Vertical dashed line in late August denotes wave event analysed in Fig. 19.

associated with peaks in the momentum fluxes—fluxes from the SH (dashed line) precede the wave events by several days, while the positive fluxes over the equator are more nearly in phase. (As a note, lag correlations calculated over the entire time period in Fig. 18 do not show significant values. However, for the 90-day period centred on July–August, maximum correlations of −0.70 [at lag −4 days] and +0.56 [at lag −1 day] are found between the wave-variance and momentum-flux time series; 5% significance is near 0.52.)

A synoptic view of the evolution of a particular wave event is shown in Fig. 19. This is the event near the end of August, noted with a dashed line in Fig. 18. Figure 19 shows the 200 mb total wind fields with no space or time filtering applied. There is initially a weak anticyclone over South America, which intensifies as a SH extratropical low to the west grows and protudes into the tropics. The extension of this wave into the tropics is accompanied by a NW–SE phase tilt (poleward momentum fluxes) which is strongest over longitudes 240–270°E near August 23 (indicated with shading in Fig. 19). The fact that the anticyclone grows initially over South America may suggest a coupling to convective activity there; note the deep vertical structure of the wave in that region (Fig. 14). There is also relatively strong northward momentum flux over the equator, associated with the north-west flank of the anticyclone in August 23–26 (also shaded in Fig. 19). Given the strong southward zonal wind shears in this location (see Fig. 12(b)), the sign of this flux is such that the wave is extracting energy from the mean flow (i.e. the flux is against the gradient, in a sense that acts to remove the background zonal wind shear). There are thus several mechanisms involved in the initial growth of the anticyclone: momentum fluxes from the SH (external, lateral forcing), possible convective coupling over South America, and *in situ* growth of wave activity at the expense of the background zonal flow.

As the anticyclone grows during August 22–24, it begins to propagate westward (which is against the background flow). As it propagates into the eastern Pacific, anticyclones appear to the east and (more clearly) to the west, and a wave-train structure is clear on August 27. Over this latter period the waves have the horizontal structure and propagation properties identified as mixed Rossby–gravity waves (see Fig. 13), although the synoptic realizations are more complex than the idealized structure.

The bursts of momentum flux from the SH extratropics are primarily associated with the decay phase of mid-latitude baroclinic-wave life cycles; such fluctuations occur continuously in the subtropics. Their proximity to the equator, and hence their ability to excite tropical waves, depends on the structure of the background zonal winds. In the case here the westerlies in the SH tropical eastern Pacific (Fig. 12(b)) allow deep meridional propagation of mid-latitude waves (as evidenced in Fig. 17). In the presence of quasi-continuous forcing from extratropics, one might expect a continuous excitation of tropical disturbances, as opposed to the events of several months' duration seen in the spectra in Fig. 6. One explanation may be the tropical regions' ability to trap meridionally-propagating waves, and more strongly excite equatorial modes. Webster and Holton (1982) and Karoly (1983) have shown that westerly wind ducts in the tropics allow interhemispheric wave propagation, whereas easterlies or near-zero winds will confine wave energy meridionally. One may thus anticipate less excitation of equatorial modes in the presence of strong westerlies.

Figure 20 shows the tropical zonal wind evolution in the form of a Hofmöller diagram during June–November 1985, together with isopleths of Rossby–gravity wave variance calculated from filtered time series (as in Fig. 12(a)). Wave events are observed in the eastern Pacific during times when the zonal winds are weak (positive or negative); note the absence of wave activity when the equatorial zonal winds are westerly (during June

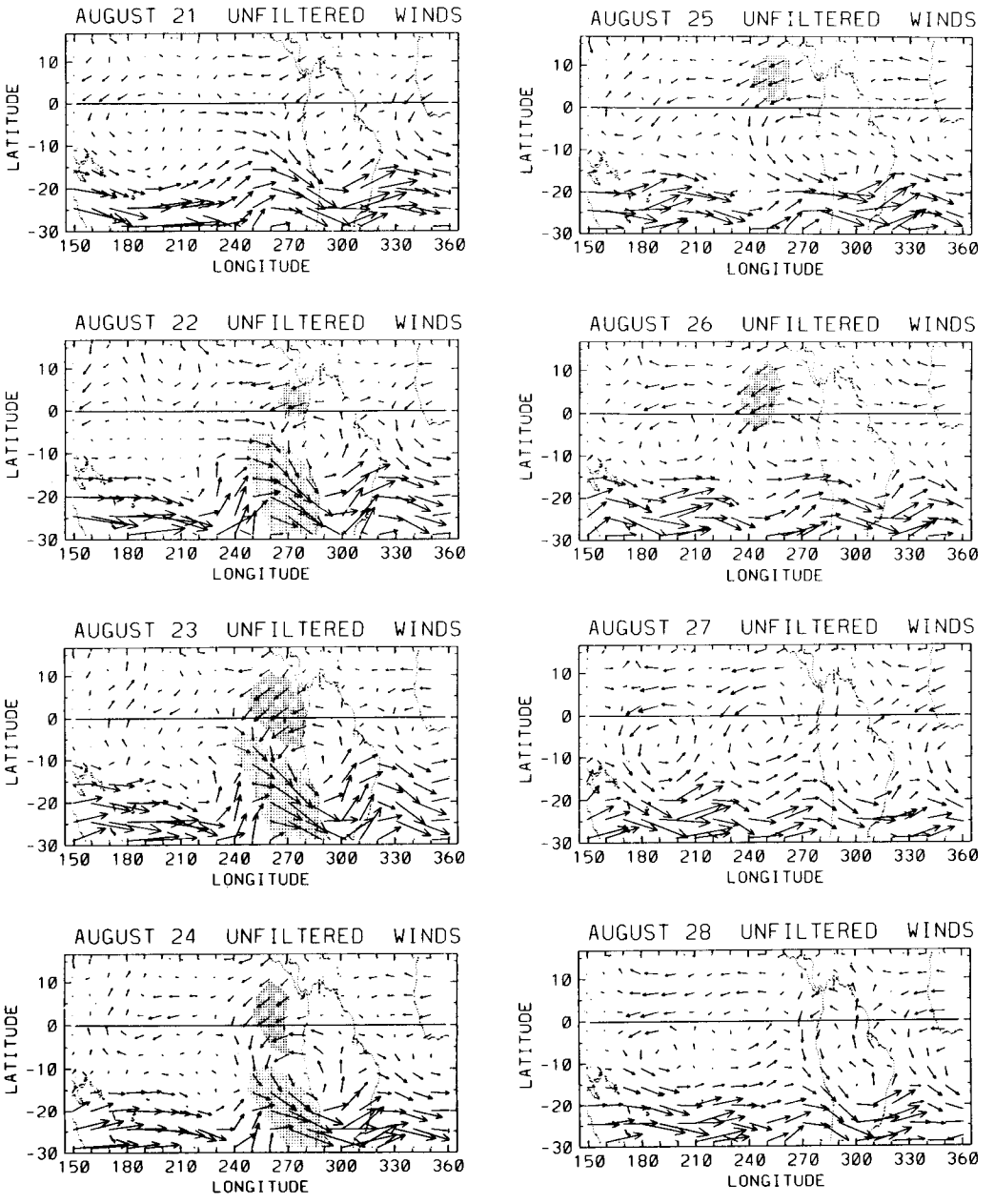

Figure 19. Latitude–longitude diagrams of the total vector winds at 200 mb over the eastern Pacific–South America region for 21–28 August 1985 (time period noted in Fig. 18). No space or time filtering has been used. Shaded areas near longitude 270°E denote regions of strong meridional momentum fluxes, as discussed in text.

and November). These data are thus consistent with a lateral forcing mechanism which requires: (1) westerlies in the subtropics to allow extratropical forcings to approach the equator, and (2) near-zero or weak easterly winds at the equator, which act to confine this wave energy and excite equatorial wave modes more strongly. We hypothesize that such configurations of the zonal wind occur occasionally, leading to the tropical wave maxima lasting for several months, as observed in Fig. 6 (although a simple time series of zonal wind does not strongly correlate with the events in Fig. 6). The eastern Pacific

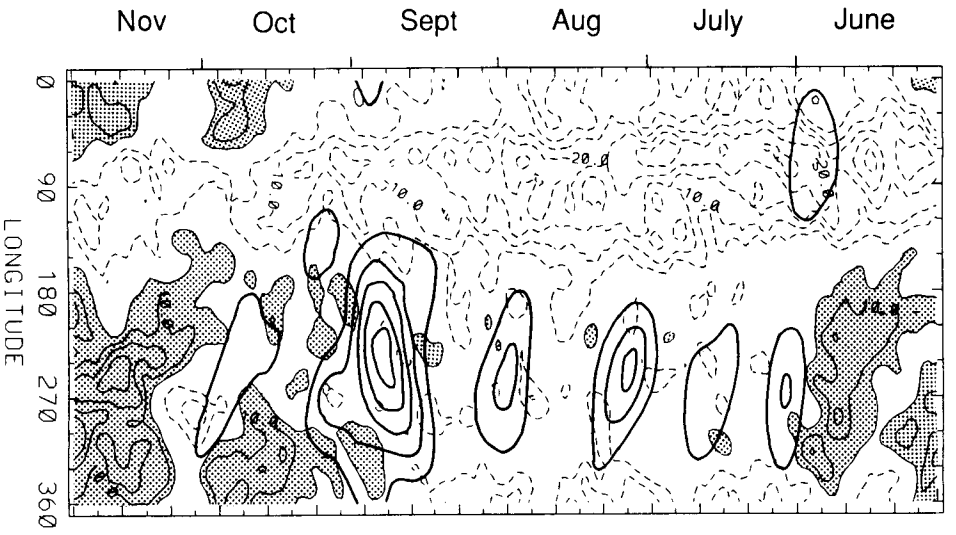

Figure 20. Hofmöller diagram of the 200 mb zonal wind averaged over 10°N–S; contours are 5 m s^{-1}, with zero contours omitted. Shading denotes westerly winds >5 m s^{-1}. Heavy contours are isopleths of westward-propagating equatorial wave variance, calculated as in Fig. 12(a). Note that equatorial waves occur only during the period of near-zero zonal winds in the western hemisphere.

is a region where low-latitude westerlies are frequently observed (Arkin and Webster 1985), and the climatological wind structure over that region is likely responsible for the occurrence of equatorially-trapped waves, particularly during August–September (see also the discussion of this region and time period in Zhang and Webster 1989, 1992).

5. Some results from CCM1

In this section brief comparisons are made with upper tropospheric waves observed in a version of CCM1. The results here come from a multi-year integration of the model using 30 vertical levels (over 0–70 km) at T-21 spectral truncation, discussed in detail in Boville and Randel (1992). Figure 21 shows zonal wave 5–6 meridional wind power over the equator at model level $\sigma = 0.245$ (approximately 245 mb) for two years of model data. Several interesting points emerge from a comparison with the observed data in Fig. 6. Firstly, there is substantially more overall wave variance at the equator in the model, primarily in quasi-stationary or eastward-moving components. This excessive model wave variance at the equator likely results from a lack of zonal mean easterlies in the model tropics (documented in Randel and Williamson 1990) that allows eastward-moving extratropical waves to propagate freely into the tropics. Secondly, the model shows evidence of westward-propagating waves with periods of 5–10 days occurring during July–August in both years in Fig. 21. The amplitude, timing and duration of these features are similar to the episodes observed in Fig. 6.

Details of the westward-propagating waves in the model are analysed from August–September of the second model year shown in Fig. 21. Figure 22(a) shows a latitude–longitude map of the meridional wind variance at $\sigma = 0.245$, synthesized from westward-propagating zonal waves 4–7 with periods of 5–13 days. Figure 22(b) shows the corresponding mean zonal wind. The patterns in Fig. 22(a) show westward-propagating variance concentrated in the western hemisphere centred near 10°S, in the region of weak westerly zonal winds. A smaller amplitude maximum is also observed over the

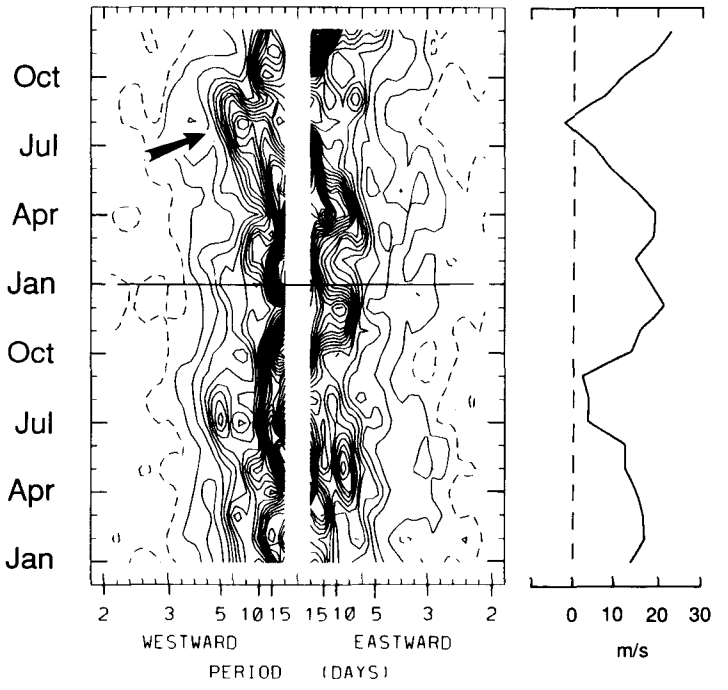

Figure 21. Power spectra for zonal wave-number 5–6 meridional wind fluctuations over the equator for model level $\sigma = 0.245$, from two years of CCM1 data. Contours are the same as in Fig. 6. Arrow in second year denotes wave event analysed in Fig. 22. Time series at right denotes zonal wind averaged over the region 3°S–8°N, 210–330°E (see Fig. 22(b)).

equator west of the date line. The horizontal and vertical structures of the westward-propagating waves in the model (not shown) are very similar to those shown for the observations in Figs. 13–14, e.g. they show the signature of Rossby–gravity modes centred south of the equator, with maximum amplitude and coherence in the upper troposphere.

Overall there is substantial similarity between the observed and modelled westward-propagating waves, notably in their longitudinally and temporally localized natures. The seasonal variation of wave spectra in CCM1 (Fig. 21) shows a strong coupling to the zonal wind near the equator. As shown in Fig. 21, the equatorial waves appear only when the background zonal winds are near zero. The absence of such waves in background westerlies (i.e. all times except July–September in Fig. 21) supports the idea of meridional trapping discussed above.

As an interesting comparison, Hamilton and Mahlman (1988) discuss the characteristics of westward-propagating waves at the 103 mb level in the GFDL 'SKYHI' model. Comparison with their results shows two notable similarities with the waves analysed here: the waves show a maximum in intensity over July–October (their Fig. 31), and their latitudinal structure exhibit a maximum near 5°S (their Fig. 27). These similar wave characteristics in observations and two model simulations suggest these are fundamental aspects of tropical wave behaviour.

6. Discussion

The comparisons with direct RAOB data have validated the utility of the ECMWF wind analyses in the tropical upper troposphere for the estimation of space–time spectra.

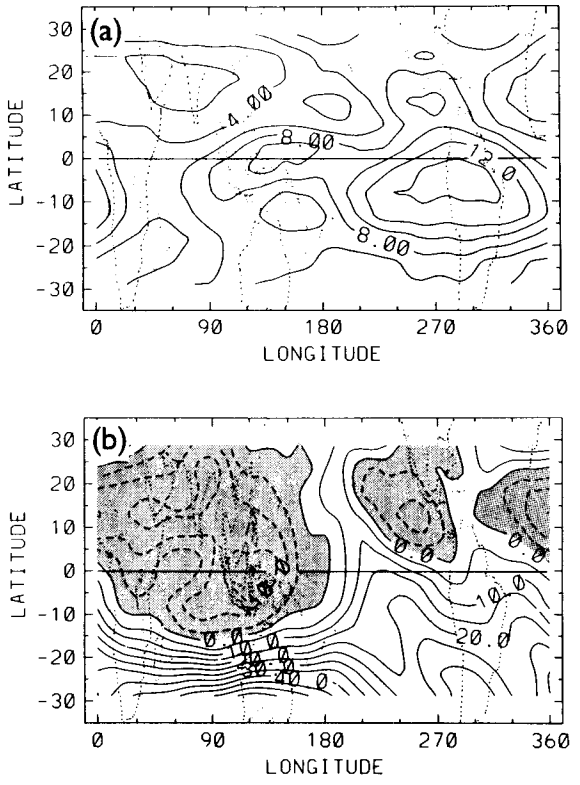

Figure 22. (a) Latitude–longitude map of the meridional wind variance in CCM1 for westward-propagating zonal waves 4–7 with periods of 5–13 days. Data are from model level $\sigma = 0.245$, taken from the second model year shown in Fig. 21. Contours are $2\,m^2s^{-2}$. (b) $\sigma = 0.245$ zonal wind from the same time period as in (a). Contours are $5\,m\,s^{-1}$, with easterlies shaded.

Meridional wind component fluctuations observed in the global analyses are seen directly in the RAOBs for two 90-day samples (one of which is shown in Figs. 15–16). Zonal wind fluctuations also show strong correlation between analyses and RAOBs, consistently higher in fact than the meridional-component correlations. The 5-day zonal wind oscillations discussed in section 3 were not evident in the RAOB spectra; this may not be surprising, however, in light of the small contribution of this mode to the total zonal wind variance.

Space–time spectra from the ECMWF data do not show distinct spectral peaks corresponding to the 10- to 20-day eastward-moving Kelvin waves or westward-propagating equatorially-trapped Rossby modes observed in Yanai and Lu (1983). Analysis of station data and satellite observations show distinct spectral peaks in the lower stratosphere for 10- to 20-day Kelvin waves (Angel *et al.* 1973; Salby *et al.* 1984); the results of Garcia and Salby (1987) demonstrate the emergence of such peaks in the lower stratosphere from random forcing in the troposphere having a red spectrum in frequency. Boville and Randel (1992) find a similar result, i.e. distinct Kelvin-wave peaks only above the tropopause level. The ECMWF zonal wind spectra show a 5-day westward-propagating wave-1 oscillation with maximum amplitude centred over the equator. This apparently corresponds to a near-global Rossby normal mode, as evidenced by coherent geopotential-height oscillations over 40°S–60°N and 0–35 km (Fig. 5(a)). This mode has been identified previously in tropospheric observations (Yanai and Lu 1983; Madden

and Julian 1972), stratospheric satellite observations (Rodgers 1976; Hirota and Hirooka 1984; Venne 1989), and a variety of models (Tsay 1974; Schoeberl and Clark 1980; Salby 1981). It is also strongly forced in the calculations of Garcia and Salby (1987); in contrast, convection centred at or near the equator failed to excite Rossby–gravity waves in their model.

Upper tropospheric meridional wind spectra over the equator show maximum variance for westward-propagating zonal waves 4–7 with periods of 6–10 days. These data reveal episodes of enhanced wave activity which persist for one to several months (Fig. 6). Most of these episodes show some degree of meridional trapping in low latitudes. The horizontal structure of these oscillations is that of Rossby–gravity waves, although they are not necessarily centred over the equator in the upper troposphere. This asymmetry with respect to the equator is possibly due to the effects of background winds; note there is a mean southward meridional wind component of order $3\,m\,s^{-1}$ over the eastern Pacific region during the period analysed in Fig. 12, which one could imagine to simply advect the Rossby–gravity modes southward. There are also substantial zonal wind shears in the region of the waves (Figs. 12(b) and 22(b)), which Boyd (1978) has shown to offset idealized Rossby–gravity waves away from the equator (although not to the degree seen here).

The upper tropospheric Rossby–gravity waves studied here are fundamentally distinct from the fast 4- to 5-day Rossby–gravity modes observed mainly in the western Pacific (Fig. 10); their differing vertical structures suggest they are forced by distinct physical mechanisms. The upper tropospheric modes are not strongly coupled with the surface, arguing against a wave-CISK mechanism for their primary excitation and maintenance. Rather, analyses of events during July–September 1985 suggest the equatorial waves are excited by meridional propagation of extratropical waves, together with *in situ* dynamical growth over the equator, and possible convective coupling over South America. Because the extratropical momentum fluxes occur first (Figs. 18–19), they may be the initial trigger. The wave number–frequency character of the equatorial-mode response is dependent on the vertical, horizontal and temporal signature of the forcing (Zhang and Webster 1992; Zhang 1992). The vertical structure of the observed forcing is equivalent barotropic with maximum amplitude near 200 mb (not shown), with slow zonal propagation. The zonal scale of the extratropical wave near 20–30°S in Fig. 19 is 60–70° longitude, i.e. zonal waves 5–6; this is close to that of the observed Rossby–gravity response (Figs. 11–13). This may suggest that the equatorial-mode wave-number spectrum is determined from that of extratropical forcing, with modal frequencies determined via the dispersion relation. This hypothesis is consistent with the climatological equatorial-wave spectra (Fig. 1) and observed eddy-momentum-flux spectra in the subtropics (Randel and Held 1991, their Fig. 3) both having maxima at zonal waves around 4–6.

The existence of the upper tropospheric waves is also closely tied to the background zonal wind structure near the equator. Given the dependence of meridional wave propagation on the structure of the background zonal winds, the observations here suggest that the excitation of upper tropospheric Rossby–gravity waves depends on: (1) westerly winds in the subtropics to allow mid-latitude waves to approach the equator, and (2) near zero or easterly winds near the equator to trap that wave energy, and strongly excite equatorial wave modes. The occasional occurrence of such conditions may explain the longitudinally and temporally localized nature of the tropical waves, in particular their frequent occurrence over the eastern Pacific in August–September.

The absorption of vertically propagating Rossby–gravity waves are proposed to be a momentum source for the westward acceleration phase of the QBO (Holton and

Lindzen 1972). The zonally-averaged magnitudes of such waves are of most direct relevance to that problem, as opposed to isolated station observations, because the QBO is observed to be zonally symmetric (Dunkerton and Delisi 1985). The ECMWF data at 100 mb are the best analyses available to estimate appropriate values for such zonally averaged results. Furthermore, seasonal and longer-term variability may be examined with these data. Regarding these latter points, Dunkerton (1990) has discussed the seasonal synchronization of the QBO westward acceleration phase, suggesting a possible explanation via a strong seasonal modulation of Rossby–gravity wave activity.

Figure 23 shows the time series over 1980–87 of westward-propagating meridional wind variance (for zonal waves 1–10) at 100 mb, averaged over 6°N–6°S, evaluated for period ranges of 2–15 days and 2–6 days. The latter high-frequency waves constitute approximately half the variance of the former at 100 mb, and may be of more relevance to the QBO problem because they propagate more readily into the lower stratosphere (e.g. Boville and Randel 1992). Variances of order 3–6 $m^2 s^{-2}$ are calculated from these data, corresponding to r.m.s. wind fluctuations of 1.7–2.4 $m s^{-1}$. Note that there is an increase in variance in mid 1986 seen in Fig. 23, which is possibly associated with the introduction of three new stratospheric levels into the ECMWF prediction model on 13 May 1986 (Trenberth and Olson 1988). After this time r.m.s. wind oscillations of 2–3 $m s^{-1}$ are observed.

Figure 23 also shows the observed zonal winds at 50 mb, and their acceleration, for comparison with the wave variance time series. The data in Fig. 23 show no apparent

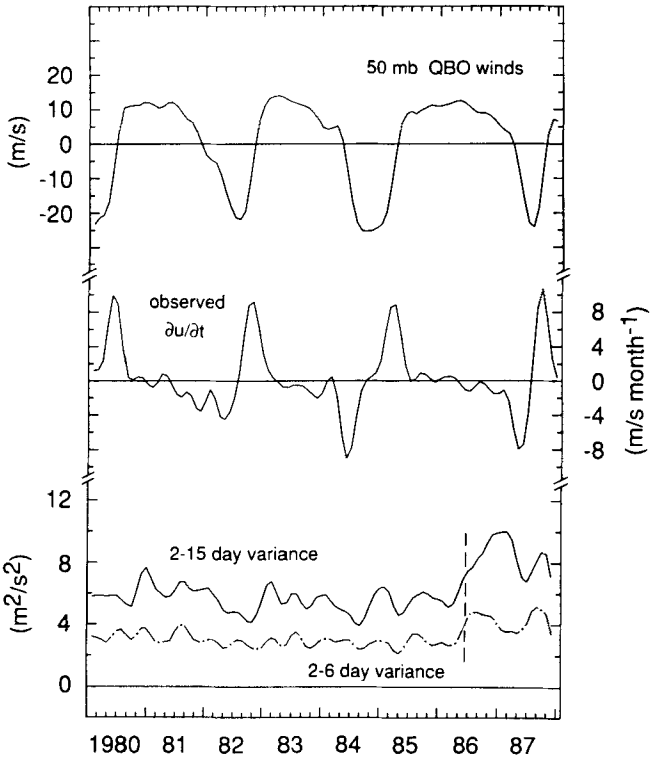

Figure 23. Bottom curves show the equatorial meridional wind variance at 100 mb for westward-propagating waves with periods 2–15 and 2–6 days for the entire data record 1980–87. The dashed line in mid 1986 denotes the introduction of three new stratospheric levels into the ECMWF prediction model, which may be related to the variance increase at that time. Top curves are the observed zonal winds at 50 mb, and their acceleration.

correlation between the observed 50 mb $\partial u/\partial t$ and wave variance at 100 mb. Furthermore, the ECMWF data do not show evidence of a strong seasonal synchronization in wave variance at 100 mb (the 8-year ensemble shows a weak maximum over July–September). These data are in basic agreement with the station RAOB analyses of Dunkerton (1991), who shows a maximum in 3- to 6-day meridional wind variance over 250 mb–100 mb during this time. Interestingly, data at 70 mb do not show a maximum at this time (see also Maruyama 1991), suggesting that the seasonal variation of Rossby–gravity wave activity in the lower stratosphere is more strongly related to background winds than to the strength of forcing from the upper troposphere.

Acknowledgements

This work has been supported under NASA grant W-16215. The data were provided by the ECMWF. Dave Baumhefner, Peter Gent, Roland Madden and Joe Tribbia provided insightful discussions. Helpful reviews were given by Byron Boville, Rolando Garcia, Kevin Trenberth, Victor Magana, Michio Yanai, and two anonymous reviewers. Marilena Stone patiently prepared the manuscript through several revisions.

References

Angel, J. K., Cotton, G. F. and Korshorer, J. 1973 A climatological analysis of oscillations of Kelvin wave period at 50 mb. *J. Atmos. Sci.*, **30,** 13–24

Arkin, P. and Webster, P. J. 1985 Annual and interannual variability in the tropical–extratropical interactions: an empirical study. *Mon. Weather Rev.*, **113,** 1510–1523

Boville, B. A. and Randel, W. J. 1992 Equatorial waves in a stratospheric GCM: effects of vertical resolution. *J. Atmos. Sci.*, in Press

Boyd, J. P. 1978 The effects of latitudinal shear on equatorial waves. Part II: Applications to the atmosphere. *J. Atmos. Sci.*, **35,** 2259–2267

Burpee, R. W. 1972 The origin and structure of easterly waves in the lower troposphere of North Africa. *J. Atmos. Sci.*, **29,** 921–925

Cats, G. J. and Wergen, W. 1982 Analysis of large scale normal modes by the ECMWF analysis system. Pp. 343–372 in *ECMWF workshop on current problems in data assimilation*

Chatfield, C. 1980 *The analysis of time series: An introduction.* 2nd edition. Chapman and Hall

Dunkerton, T. J. 1985 A two-dimensional model of the quasi-biennial oscillation. *J. Atmos. Sci.*, **42,** 1151–1160

1990 Annual variation of deseasonalized mean flow acceleration in the equatorial lower stratosphere. *J. Meteorol. Soc. Japan*, **68,** 499–508

1991 Intensity variation and coherence of 3–6 day equatorial waves. *Geophys. Res. Lett.*, **18,** 1469–1472

Dunkerton, T. J. and Delisi, D. P. 1985 Climatology of the equatorial lower stratosphere. *J. Atmos. Sci.*, **42,** 376–396

Garcia, R. R. and Salby, M. L 1987 Transient response to localized episodic heating in the tropics. Part II: Far field behaviour. *J. Atmos. Sci.*, **44,** 499–530

Hamilton, K. and Mahlman, J. D. 1988 General circulation model simulation of the semi-annual oscillation of the tropical middle atmosphere. *J. Atmos. Sci.*, **45,** 3212–3235

Hayashi, Y. 1982 Space–time spectral analysis and its application to atmospheric waves. *J. Meteorol. Soc. Japan*, **60,** 156–171

Heckley, W. A. 1985 Systematic errors of the ECMWF operational forecasting model in the tropical regions, *Q. J. R. Meteorol. Soc.*, **111,** 709–738

Hendon, H. H. and Liebman, B. 1991 The structure and annual variation of antisymmetric fluctuations of tropical convection and their association with Rossby–gravity waves. *J. Atmos. Sci.*, **48,** 2127–2140

Hirota, I. and Hirooka, T. 1984 Normal mode Rossby waves observed in the upper stratosphere. Part I: First symmetric modes of zonal wave numbers 1 and 2. *J. Atmos. Sci.*, **41**, 1253–1267

Holton, J. R. and Lindzen, R. S. 1972 An updated theory for the quasi-biennial cycle of the tropical stratosphere. *J. Atmos. Sci.*, **29**, 1076–1080

Itoh, H. and Ghil, M. 1988 The generation mechanism of mixed Rossby–gravity waves in the equatorial troposphere. *J. Atmos. Sci.*, **45**, 585–604

Karoly, D. J. 1983 Rossby wave propagation in a barotropic atmosphere. *Dyn. Atmos. Oceans*, **7**, 111–125

Liebman, B. and Hendon, H. H. 1990 Synoptic-scale disturbances near the equator. *J. Atmos. Sci.*, **47**, 1463–1479

Madden, R. A. and Julian, P. R. 1972 Further evidence of global-scale 5-day pressure waves. *J. Atmos. Sci.*, **29**, 1464–1469

Magaña, V. and Yanai, M. 1991 Equatorial modes in the upper troposphere. Pp. 461–466 in Preprint volume, *19th Conference on Hurricanes and Tropical Meteorology*. American Meteorological Society

Maruyama, T. 1979 Equatorial wave intensity over the Indian Ocean during the years 1968–1972. *J. Meteorol. Soc. Japan*, **57**, 39–50

1991 Annual and QBO-synchronized variations of lower-stratospheric equatorial wave activity over Singapore during 1961–1989. *J. Meteorol. Soc. Japan*, **69**, 219–231

Matsuno, T. 1966 Quasi-geostrophic motions in the equatorial area. *J. Meteorol. Soc. Japan*, **44**, 25–42

Nitta, T. 1970 Statistical study of tropospheric wave disturbances in the tropical Pacific region. *J. Meteorol. Soc. Japan*, **48**, 47–59

Pedlosky, J. 1979 *Geophysical fluid dynamics*. Springer-Verlag, New York

Randel, W. J. and Held, I. M. 1991 Phase speed spectra of transient eddy fluxes and critical layer absorption. *J. Atmos. Sci.*, **48**, 688–697

Randel, W. J. and Williamson, D. L. 1990 A comparison of the climate simulated by the NCAR Community Climate Model (CCM1:R15) with ECMWF analyses. *J. Climate*, **3**, 608–633

Rodgers, C. D. 1976 Evidence for the 5-day wave in the upper stratosphere. *J. Atmos. Sci.*, **33**, 710–711

Salby, M. L. 1981 Rossby normal modes in nonuniform background configurations, Part II: Equinox and solstice conditions. *J. Atmos. Sci.*, **38**, 1827–1840

Salby, M. L., Hartmann, D. L., Gille, J. C. and Bailey, P. L. 1984 Evidence of equatorial Kelvin modes in Nimbus-7 LIMS. *J. Atmos. Sci.*, **41**, 220–235

Schoeberl, M. L. and Clark, J. H. E. 1980 Resonant planetary waves in a spherical atmosphere. *J. Atmos. Sci.*, **37**, 20–28

Tai, K.-S. and Ogura, Y. 1987 An observational study of easterly waves over the eastern Pacific in the northern summer using FGGE data. *J. Atmos. Sci.*, **44**, 339–361

Trenberth, K. E. and Olson, J. G. 1988 An evaluation and intercomparison of global analyses from the National Meteorological Center and the European Centre for Medium Range Weather Forecasts. *Bull. Am. Meteorol. Soc.*, **69**, 1047–1057

Tsay, C.-Y. 1974 Analysis of large-scale wave disturbances in the tropics simulated by an NCAR global circulation model. *J. Atmos. Sci.*, **31**, 330–339

Venne, D. E. 1989 Normal mode Rossby waves observed in the wave number 1–5 geopotential fields of the stratosphere and troposphere. *J. Atmos. Sci.*, **46**, 1042–1056

Wallace, J. M. 1971 Spectral studies of tropospheric wave disturbances in the tropical western Pacific. *Rev. Geophys. Space Phys.*, **9**, 557–612

Webster, P. J. and Holton, J. R. 1982 Cross-equatorial response to middle-latitude forcing in a zonally varying basic state. *J. Atmos. Sci.*, **39**, 722–733

Yanai, M. and Lu, M.-M. 1983 Equatorially trapped waves at the 200 mb level and their association with meridional convergence of wave energy flux. *J. Atmos. Sci.*, **40**, 2785–2803

Yanai, M. and Maruyama, T. 1966 Stratospheric wave disturbances propagating over the equatorial Pacific. *J. Meteorol. Soc. Japan*, **44**, 291–294

Yanai, M. and Murakami, M. 1970 A further study of tropical wave disturbances by the use of spectrum analysis. *J. Meteorol. Soc. Japan*, **48**, 185–197

Zangvill, A. 1977 On the presentation and interpretation of spectra of large scale disturbances. *Mon. Weather Rev.*, **105**, 1469–1472

Zangvill, A. and Yanai, M. 1980 Upper tropospheric waves in the tropics. Part I: Dynamical analysis in the wave number–frequency domain. *J. Atmos. Sci.*, **37**, 283–298

Zhang, C. 1992 Laterally forced equatorial perturbations in a linear model. Part II: Mobile forcing. *J. Atmos. Sci.*, in Press

Zhang, C. and Webster, P. J. 1989 Effects of zonal flows on equatorially trapped waves. *J. Atmos. Sci.*, **46**, 3632–3652

1992 Laterally forced equatorial perturbations in a linear model. Part I: Stationary transient forcing. *J. Atmos. Sci.*, in Press

Ziemke, J. R. and Stanford, J. L. 1990 One-to-two-month oscillations in the stratosphere during southern winter. *J. Atmos. Sci.*, **47**, 1778–1793